Optimal control of a wind-PV-hybrid powered heat pump water heater[1]

Sam Sichilalu*, Tebello Mathaba, Xiaohua Xia

Centre of New Energy Systems, Department of Electrical, Electronic and Computer Engineering, University of Pretoria, Pretoria 0002, South Africa

Abstract

This paper develops an optimal control (OC) model of a heat pump water heater (HPWH) supplied by a wind generator-photovoltaic-grid system. The objective function is energy cost minimization, taking into account the time-of-use electricity tariff (TOU), which is an important control parameter. The control variables are the supply switch to the HPWH and the power from the grid, while the hot water temperature inside the tank is the state variable. The model meets both the HPWH's technical and operational constraints in providing hot water at a desired temperature and achieves load shifting. This problem is solved using a mixed integer linear program. The results show a 70.7% cost reduction upon implementation of this intervention. A case study is done and the OC shows significant potential in energy and cost saving when compared to the digital thermostat controller used currently in most HPWHs. The economic analysis is presented in this paper as well.

Keywords: Heat pump water heater; Optimal switching control; Photovoltaic; Wind generator; Time-of-use tariff; Mixed integer linear program.

[1]This paper was presented at the 7th International Conference on Applied Energy (ICAE2015), March 28-31, 2015, Abu Dhabi, UAE (Original paper title: "Optimal power control of grid tied PV-battery-diesel system powering heat pump water heaters" and Paper No.: 66).

*Corresponding author. Tel. +27 12 420 6767; Fax +27 12 362 5000.

Email address: Sam.Sichilalu@up.ac.za ; sichgroup@yahoo.com (Sam Sichilalu)

Nomenclature	
$P_w(t)$	wind generator power output (kW)
$P_{pv}(t)$	photovoltaic power output (kW)
$P_g(t)$	grid power (kW)
P_{hp}	heat pump water heater power demand (kW)
COP	coefficient of performance
$u(t)$	heat pump power supply switch control variable (0 or 1)
$T(t)$	hot water temperature inside the tank ($^\circ$C)
T_{low} and T_{up}	lower and upper hot water temperature set points ($^\circ$C)
T_a	ambient temperature ($^\circ$C)
T_o	initial hot water temperature ($^\circ$C)
$T_{in}(t)$	inlet cold water temperature ($^\circ$C)
R	South African Rands (ZAR)
$p(t)$	time-of-use electricity price (R/kWh)
N	total number of sampling intervals
t_s and k	sampling time ($hour$) and k^{th} sampling interval
Q_D	total losses due to water demand
Q_L	total standby (convectional) losses
$W_D(t)$	flow rate ($litres/hour$)
q_{loss}	conventional loss in (W/m^2)
$\triangle x$	thickness of the insulation (m)
h	surface heat transfer coefficient (W/m^2K)
κ	thermal conductivity ($W/m\ K$)
S_{area}	total surface area (m^2)
c	specific heat capacity of water ($J/kg\,^\circ$C)
$\dot{T}$	derivative of temperature
L	mass of water inside the tank (kg)
η_t	turbine coupling gearbox efficiency (%)
η_g	wind generator efficiency (%)
ρ	air density factor of the wind generator
C_p	Betz limit
A_w	wind generator rotor sweeping area (m^2)
V_r	wind velocity (m/s)
DPV	discounted present value of the future cash flow
FV	nominal value of a cash flow amount in a future period
r	interest rate or discount rate
n	time in years before the future cash flow occurs
MILP	Mixed Integer Linear Program

1. Introduction

The energy consumption in buildings accounts for about 42% of global energy production, especially in developed countries [1]; 60.51% of this energy goes for space heating and 23.60% for water heating at domestic[2] level. Therefore, in order to reduce the high energy consumption, energy-efficient equipment, such as heat pump water heaters (HPWH), needs to be employed at domestic level as tools for demand side management (DSM). HPWHs are devices that drive heat energy from a cooler surrounding medium to a much warmer place using a refrigerant. The refrigerant absorbs the ambient energy of the surrounding medium in the evaporator and passes through the compressor, where it gains extra heat energy through an

[2]http://www.dti.gov.uk/energy/inform/

increase in pressure as a result of compression. This hot working fluid then circulates through the heat exchanger (condenser), where thermal energy is transferred to the water and the process is repeated. The past two decades have seen major advances in HPWH technology [2, 3, 4], which has led to their wider application and improved coefficient of performance (COP). Essen and Yuksel [5] extensively investigated both ground-sourced and air-sourced HPWHs and made an economic analysis. Various authors [6, 7, 8, 9, 10, 11] have developed models and investigated ways of improving the COP of the HPWH; however, most of them agree that optimal control (OC), system design, sizing and integration remain a technological challenge.

The problem of DSM requires a multi-directional approach; the HPWHs alone might not achieve significant energy savings, hence the need to integrate them with distributed renewable energy sources (DREs) such as wind and photovoltaic (PV) power in buildings [12, 13]. On/off-site DRE integration into buildings and small communities is a promising technology for DSM. Various hybrid DREs are presented in [14, 15, 16, 17, 18, 19, 20], though much of the success achieved so far is in the sizing and system design. More effort and research are required to integrate these DREs optimally into energy-efficient household loads (e.g. heat pumps) to realize net-zero energy [21], cost-effective billing and positive-energy buildings [22]. Therefore, future optimal energy-mixing will rely on the successful implementation of OC techniques [23, 24**?**].

This paper proposes the first attempt to provide an optimal switching control model of the HPWH, supplied by wind-PV-grid hybrid systems, that save energy and cost in practice. Many previous works evaluate the techno-economic benefit [25, 26, 27, 28, 29, 30, 31], i.e, the objective functions are performances over a year, or multiple years. Operational performances are evaluated at a much shorter period, such as a day, 24h. A control horizon of one day enable end-users to effectively monitor their daily energy usage. The daily savings will accumulate into savings over weeks, months, seasons and years allowing end-users to easily understand their daily energy consumption trends and their cost implications. This is a major difference. This model meets both the technical and operational constraints of an HPWH powered by DREs and meets the required hot water demand at a desirable temperature, which is another novelty of this paper. The model further shows the potential of achieving a cost-effective and near net-zero energy building. The limitations of the current digital thermostat temperature controller used in HPWH can be alleviated by the application of the OC. This model can also be adopted for optimal renewable energy feed-in by building owners intending to achieve positive-energy and cost-effective consumption.

This paper is structured as follows: Sections 2 and 3 present the mathematical model formulation and Section 4 the simulation results and discussion. The last part, Section 5, is the conclusion.

2. Mathematical model formulation

2.1. Schematic model layout

The optimal switching strategy schematic diagram of the heat pump shown in Figure 1 comprises the wind generator $P_w(t)$, PV modules $P_{pv}(t)$, grid $P_g(t)$ and an air-sourced heat pump with tank-wrapped condenser $P_{hp}(t)$. The switch $u(t)$ controls the power supply to the HPWH. The excess renewable power is fed into the grid. The grid power $P_g(t)$ accepts power from renewable power sources as well as it supplements the heat pump whenever their combined output fails to meet the demand.

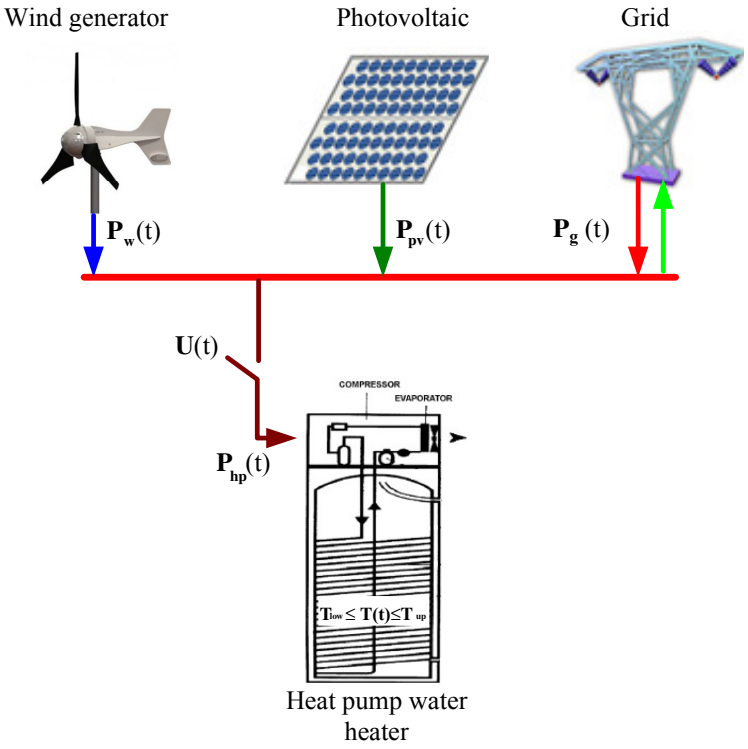

Figure 1: Schematic layout of the model.

The time-of-use electricity tariff (TOU) is one of the important control parameters in the optimal switching strategy of the HPWH, especially in the peak period. $T(t)$ is the state variable, the temperature of the water inside the storage tank. The hot water demand $W_D(t)$ is the flow rate in litres/hour taken from the case study. The desired hot water temperature is predetermined to lie between T_{low} and T_{up}, which are the lower and upper temperature respectively. However, these limits may vary from one individual to another. The control variables in this paper are the grid power $P_g(t)$ and heat pump supply switch $u(t)$.

2.2. Sub-models

2.2.1. Heat pump water heater

The heat pump model is developed according to [32], with a fixed power demand P_{hp} rating, operating at full capacity. The temperature distribution of the hot water is assumed to be uniform and with a constant water volume, neglecting stratification. The energy loss in the evaporator, refrigerant and compressor is not considered in this model because it is negligible. Therefore, only energy losses due to the hot water demand $Q_D(t)$ and convectional (standby) loss $Q_L(t)$ are taken into account.

The standby $Q_L(t)$ are the thermal losses dispatched through the tank's casing material. These losses can be minimised through increased thermal insulation and application of low thermal conductivity materials. The per second convention loss q_{loss} in W/m^2 according to [33] is given in equation (1),

$$q_{loss}\left(T(t), T_a\right) = \frac{T(t) - T_a}{\frac{\triangle x}{\kappa} + \frac{1}{h}}, \tag{1}$$

where $\triangle x$ and κ are the insulation thickness and thermal conductivity coefficients respectively, h is the surface heat transfer coefficient of the tank, $T(t)$, T_a are the hot water and ambient temperature respectively. Therefore, for a given tank surface area S_{area}, the total standby losses are:

$$Q_L\left(T(t), T_a\right) = q_{loss} S_{area}. \tag{2}$$

The other loss is associated with the hot water demand $Q_D(t)$, which triggers the inlet cold water into the tank to maintain volume. $T(t)$ is expected to drop during demand because of the inlet of cold water into the tank. The losses associated with the hot water demand are given as [34, 35] in equation (3):

$$Q_D(t) = cW_D(t)\left(T(t) - T_{in}\right), \tag{3}$$

where $c = 4180J/kg/\,^{\circ}\mathrm{C}$ is the specific heat capacity of water. T_{in} is the municipal inlet water temperature whereas $W_D(t)$ is the flow rate in litres/hour.

Therefore, in order to satisfy the HPWH thermal output requirements, the corresponding electrical power input is [9, 34]:

$$P_{hp}(t) = \frac{Q_D(t) + Q_L(t)}{COP}. \tag{4}$$

The power balance is a dynamic equation. Let $Q_H(t)$ be the total HPWH heat output kilowatts and L the water mass in kilograms. Therefore, the power balance becomes a first derivative differential function given in equation (5) [36].

$$cL\dot{T}(t) = Q_H(t) - Q_L(t) - Q_D(t), \tag{5}$$

$$Q_H(t) = P_{ph}COPu(t). \tag{6}$$

By substituting equation (1) to (4) into equation (5), one gets

$$\dot{T}(t) = \frac{P_{ph}COPu(t) - S_{area}\left(\frac{T(t)-T_a}{\frac{\triangle x}{\kappa}+\frac{1}{h}}\right) - cW_D(t)\left(T(t) - T_{in}(t)\right)}{cL}, \tag{7}$$

denoting:

$$\alpha(t) = \frac{S_{area}}{cL\left(\frac{\triangle x}{\kappa} + \frac{1}{h}\right)} + \frac{W_D(t)}{L}, \tag{8}$$

$$\beta = \frac{P_{hp}COP}{cL}, \tag{9}$$

$$\gamma(t) = \frac{S_{area}T_a}{cL\left(\frac{\triangle x}{\kappa} + \frac{1}{h}\right)} + \frac{W_D(t)T_{in}(t)}{L}, \tag{10}$$

then equation (7) becomes:

$$\dot{T}(t) = -\alpha(t)T(t) + \beta u(t) + \gamma(t). \tag{11}$$

2.2.2. Wind generator

The wind power output is given in equation (12) where the wind velocity is taken from the case study [37, 18]. The excess wind power is fed into the grid using the established wind energy feed-in tariff.

$$P_w(t) = \eta_t\eta_g 0.5\rho_a C_p A_w V_r^3, \tag{12}$$

where η_t and η_g are the mechanical gearbox and generator efficiency respectively, ρ is the air density factor, C_p is the turbine power coefficient (Betz limit), A_w is the turbine rotor sweeping area and lastly V_r is the wind velocity. η_t and η_g are deduced through a quadratic fit into the manufacturer's data.

2.2.3. Photovoltaic power

The PV power generation $P_{pv}(t)$, which is input data in this model, is a variable power source from zero to its maximum rated value written in equation (13). The PV supplies $P_{pv}(t)$ to the HPWH and the excess is sold to the grid at the prevailing feed-in tariff. This model excludes the energy storage system in order to lower the initial investment costs, which hampers the implementation of these systems at household level. The grid therefore acts as energy storage.

$$0 \leq P_{pv}(t) \leq P_{pv}^{max}. \tag{13}$$

2.2.4. Grid power

The grid is modeled as an infinite busbar capable of simultaneously supplying and accepting power from the solar PV and wind generator. The TOU electricity tariff is one of the most important OC parameters. In South Africa, Eskom is the main power supply utility company and has both flat and dynamic pricing rates $p(t)$ or rather a TOU electricity tariff. In this model the TOU electricity tariff is considered: off-peak (p_o), standard (p_s) and peak (p_p). The recent Eskom [3] megaflex active energy-TOU tariff is incorporated as a control parameter. The Eskom TOU electricity tariff is:

$$p(t) = \begin{cases} p_o = 0.3656\text{R/kWh} & \text{if } t \in [0,7] \cup [23,24], \\ p_s = 0.6733\text{R/kWh} & \text{if } t \in [7,8] \cup [11,19] \cup [21,23], \\ p_p = 2.2225\text{R/kWh} & \text{if } t \in [8,11] \cup [19,21], \end{cases} \tag{14}$$

where R is the South African rand and t is the time of the day with $t = 0, \ldots, 23$.

The grid can accept the excess power from wind and PV, as well as complement the renewable resources in meeting the heat pump load. The power balance is written as:

$$P_{hp}u(t) - P_g(t) = P_w(t) + P_{pv}(t). \tag{15}$$

3. Discrete model formulation

3.1. Discretized hot water temperature

The water demand flow rate $W_D(t)$ and the inlet water, $T_{in}(t)$, are functions of time taken from the case study. The general discrete formulation of equation (11) in terms of the *k-th* hot water temperature is given in equation (16):

$$T_{k+1} = (1 - t_s\alpha_k)T_k + t_s\beta u_k + t_s\gamma_k. \tag{16}$$

Therefore, T_{k+1} at each interval can be derived as:

$$\begin{aligned} T_1 =& (1 - t_s\alpha_0)T_o + t_s\beta u_0 + t_s\gamma_0, \\ T_2 =& [(1 - t_s\alpha_1)(1 - t_s\alpha_0)]T_o + t_s\beta\left[(1 - t_s\alpha_1)u_0 + u_1\right] + \left[(1 - t_s\alpha_1)t_s\gamma_0 + t_s\gamma_1\right], \\ T_3 =& [(1 - t_s\alpha_2)(1 - t_s\alpha_1)(1 - t_s\alpha_0)]T_o + t_s\beta\left[(1 - t_s\alpha_2)(1 - t_s\alpha_1)u_0 + (1 - t_s\alpha_2)u_1 + u_2\right] \\ &+ \left[(1 - t_s\alpha_2)(1 - t_s\alpha_1)t_s\gamma_0 + (1 - t_s\alpha_2)t_s\gamma_1 + t_s\gamma_2\right], \\ &\vdots \\ T_{k+1} =& T_o\prod_{j=0}^{k}\left(1 - t_s\alpha_j\right) + t_s\beta\sum_{j=0}^{k}u_j\prod_{i=j+1}^{k}(1 - t_s\alpha_i) + \sum_{j=0}^{k}t_s\gamma_j\prod_{i=j+1}^{k}(1 - t_s\alpha_i), \end{aligned} \tag{17}$$

where; T_o and T_k are the initial and *k-th* water temperatures inside the tank respectively. t_s is the sampling time, whereas u_k is the *k-th* switch status, which is either 1 or 0. The acceptable hot water temperature set points are given in inequality (18):

[3] http://www.eskom.co.za/

$$T_{low} \leq T_k \leq T_{up}, \tag{18}$$

where, T_{low} and T_{up} are the lower and upper desired temperatures respectively.

3.2. Objective function

The objective function is the grid energy cost minimization under the TOU tariff in discrete time. The control horizon is one day, with t_s being the sampling time and the sampling interval is ($1 \leq k \leq N$). Objective function:

$$J = t_s \sum_{k=1}^{N} P_{g,k} p_k, \tag{19}$$

subject to the following constraints:

$$T_{low} \leq T_o \prod_{j=0}^{k} \left(1 - t_s \alpha_j\right) + t_s \beta \sum_{j=0}^{k} u_j \prod_{i=j+1}^{k} (1 - t_s \alpha_i) + \sum_{j=0}^{k} t_s \gamma_j \prod_{i=j+1}^{k} (1 - t_s \alpha_i) \leq T_{up}, \tag{20}$$

$$P_{hp} u_k - P_{g,k} = P_{w,k} + P_{pv,k}, \tag{21}$$

$$0 \leq P_{pv,k} \leq P_{pv}^{max}, \tag{22}$$

$$0 \leq P_{w,k} \leq P_{w}^{rated}, \tag{23}$$

$$u_k \in \{0, 1\}, \tag{24}$$

where p_k is the TOU electricity tariff (R/kWh) at the *k-th* sampling interval.

3.3. Algorithm formulation

The proposed model has a binary variable and real number control variables, solved using the *OPTI toolbox* SCIP algorithm in MATLAB.

3.3.1. Inequality matrices

The general formulation of the inequality constraint is shown in equation (25):

$$\mathbf{AX} \leq \mathbf{b}. \tag{25}$$

Vector $\mathbf{X}$ comprises all the control variables: switch u_k and grid power P_g written in equation (27). Let matrix $\mathbf{A}$ and vector $\mathbf{b}$ be:

$$\mathbf{A} = \begin{bmatrix} \mathbf{A_1} \\ -\mathbf{A_1} \end{bmatrix}, \qquad \mathbf{b} = \begin{bmatrix} \mathbf{b_1} \\ \mathbf{b_2} \end{bmatrix}, \tag{26}$$

and,

$$\mathbf{X} = \begin{bmatrix} u_0 \\ \vdots \\ u_{N-1} \\ P_{g,0} \\ \vdots \\ P_{g,N-1} \end{bmatrix}_{2N \times 1}. \tag{27}$$

Then matrix $\mathbf{A_1}$ is an $N \times 2N$ matrix given in equation (28):

$$\mathbf{A_1} = t_s\beta \left[\begin{array}{ccccccc:ccc} 1 & 0 & 0 & 0 & \dots & 0 & 0 & \dots & 0 \\ (1-t_s\alpha_1) & 1 & 0 & 0 & \dots & 0 & 0 & \dots & 0 \\ (1-t_s\alpha_2)(1-t_s\alpha_1) & (1-t_s\alpha_2) & 1 & 0 & \dots & 0 & 0 & \dots & 0 \\ \vdots & \vdots & \vdots & \ddots & \vdots & \vdots & 0 & \dots & 0 \\ (1-t_s\alpha_{N-2})\times\ldots\times(1-t_s\alpha_1) & (1-t_s\alpha_{N-2})\times\ldots\times(1-t_s\alpha_2) & \dots & \dots & 1 & 0 & 0 & \dots & 0 \\ (1-t_s\alpha_{N-1})(1-t_s\alpha_{N-2})\times\ldots\times(1-t_s\alpha_1) & (1-t_s\alpha_{N-1})\times\ldots\times(1-t_s\alpha_2) & \dots & \dots & (1-t_s\alpha_{N-1}) & 1 & 0 & \dots & 0 \end{array}\right], \tag{28}$$

inequality (20) is reformulated into inequality (29) and inequality (30):

$$t_s\beta \sum_{j=0}^{k} u_j \prod_{i=j+1}^{k} (1-t_s\alpha_i) \le T_{up} - T_o \prod_{j=0}^{k} \left(1-t_s\alpha_j\right) - \sum_{j=0}^{k} t_s\gamma_j \prod_{i=j+1}^{k} (1-t_s\alpha_i), \tag{29}$$

$$-t_s\beta \sum_{j=0}^{k} u_j \prod_{i=j+1}^{k} (1-t_s\alpha_i) \le -T_{low} + T_o \prod_{j=0}^{k} \left(1-t_s\alpha_j\right) + \sum_{j=0}^{k} t_s\gamma_j \prod_{i=j+1}^{k} (1-t_s\alpha_i). \tag{30}$$

According to inequality (29) and inequality (30), the element of vectors $\mathbf{b_1}$ and $\mathbf{b_2}$ are:

$$b_{1,k} = T_{up} - T_o \prod_{j=0}^{k} \left(1-t_s\alpha_j\right) - \sum_{j=0}^{k} t_s\gamma_j \prod_{i=j+1}^{k} (1-t_s\alpha_i), \tag{31}$$

$$b_{2,k} = -T_{low} + T_o \prod_{j=0}^{k} \left(1-t_s\alpha_j\right) + \sum_{j=0}^{k} t_s\gamma_j \prod_{i=j+1}^{k} (1-t_s\alpha_i). \tag{32}$$

Vector $\mathbf{b_1}$ in equation (31) is the difference in three vectors $\mathbf{b_3}$, $\mathbf{b_4}$ and $\mathbf{b_5}$, as shown in equation (33).

$$\mathbf{b_1} = \mathbf{b_3} - \mathbf{b_4} - \mathbf{b_5}, \tag{33}$$

where,

$$\mathbf{b_3} = \begin{bmatrix} T_{up} \\ \vdots \\ T_{up} \end{bmatrix}_{N\times 1}, \tag{34}$$

then vector $\mathbf{b_4}$ is given in equation (35),

$$\mathbf{b_4} = T_o \begin{bmatrix} (1-t_s\alpha_0) \\ (1-t_s\alpha_1)(1-t_s\alpha_0) \\ (1-t_s\alpha_2)(1-t_s\alpha_1)(1-t_s\alpha_0) \\ \vdots \\ (1-t_s\alpha_{N-2})(1-t_s\alpha_{N-3})\times\ldots\times(1-t_s\alpha_0) \\ (1-t_s\alpha_{N-1})(1-t_s\alpha_{N-2})(1-t_s\alpha_{N-3})\times\ldots\times(1-t_s\alpha_0) \end{bmatrix}_{N\times 1}, \tag{35}$$

and finally, $\mathbf{b_5}$ is given in equation (36) below,

$$\mathbf{b_5} = \begin{bmatrix} t_s\gamma_o \\ (1-t_s\alpha_1)t_s\gamma_o + t_s\gamma_1 \\ (1-t_s\alpha_2)(1-t_s\alpha_1)t_s\gamma_o + (1-t_s\alpha_2)t_s\gamma_1 + t_s\gamma_2 \\ \vdots \\ (1-t_s\alpha_{N-2})\times\ldots\times(1-t_s\alpha_1)t_s\gamma_o + (1-t_s\alpha_{N-2})\times\ldots\times(1-t_s\alpha_2)t_s\gamma_1 + \ldots + t_s\gamma_{N-2} \\ (1-t_s\alpha_{N-1})(1-t_s\alpha_{N-2})\times\ldots\times(1-t_s\alpha_1)t_s\gamma_o + (1-t_s\alpha_{N-1})\times\ldots\times(1-t_s\alpha_2)t_s\gamma_1 + \ldots(1-t_s\alpha_{N-1})t_s\gamma_{N-2} + t_s\gamma_{N-1} \end{bmatrix}. \tag{36}$$

The T_{low} vector is given in equation (37), the formulation of $\mathbf{b_2}$ vector is analogous to $\mathbf{b_1}$ given in equation (38),

$$\mathbf{b_6} = \begin{bmatrix} T_{low} \\ \vdots \\ T_{low} \end{bmatrix}_{N\times 1}, \tag{37}$$

$$\mathbf{b_2} = -\mathbf{b_6} + \mathbf{b_4} + \mathbf{b_5}. \tag{38}$$

3.3.2. Equality matrices

The power balance equation (15) constitutes an equality constraint, a sparse matrix $\mathbf{A_{eq}}$, given in equation (39):

$$\mathbf{A_{eq}} = \begin{bmatrix} P_{hp} & 0 & \cdots & 0 & \vdots & -1 & 0 & \cdots & 0 \\ 0 & P_{hp} & 0 & \cdots & \vdots & 0 & \ddots & \cdots & 0 \\ \vdots & 0 & \ddots & 0 & \vdots & \vdots & 0 & -1 & \vdots \\ 0 & 0 & \cdots & P_{hp} & \vdots & 0 & 0 & \cdots & -1 \end{bmatrix}_{N\times 2N}. \tag{39}$$

The *k-th* total PV and wind power constitute element of vector $\mathbf{b_{eq}}$ is shown in equation (40):

$$\mathbf{b_{eq}} = \begin{bmatrix} P_{w,1} + P_{pv,1} \\ \vdots \\ P_{w,N} + P_{pv,N} \end{bmatrix}_{N\times 1}. \tag{40}$$

Therefore, the canonical form is $\mathbf{A_{eq}X} = \mathbf{b_{eq}}$ where $\mathbf{A_{eq}}$ is given in equation (39) and $\mathbf{b_{eq}}$ in equation (40).

3.3.3. The objective function

The objective function is the total daily electrical energy cost under the TOU tariff given by,

$$f^T X = \begin{bmatrix} 0 & \dots & 0_N, & p_1 & \dots & p_N \end{bmatrix} \begin{bmatrix} u_0 \\ \vdots \\ u_{N-1} \\ P_{g,0} \\ \vdots \\ P_{q,N-1} \end{bmatrix}_{2N\times 1} . \tag{41}$$

The limits of the control variables are restricted between the lower and upper bounds, given in equation (42) and equation (43).

lower bounds

$$lb^T = \begin{bmatrix} 0 & \dots & 0_N, & -\infty_1 & \dots & -\infty_N \end{bmatrix}, \tag{42}$$

upper bounds

$$ub^T = \begin{bmatrix} 1 & \dots & 1_N, & \infty_1 & \dots & \infty_N \end{bmatrix}. \tag{43}$$

3.4. Case study

The case study is based on a farmhouse situated in the peripheral town of Port Elizabeth in South Africa. The major intervention of this model proposes an optimal control and renewable power integration solution to the HPWH installed at this farmhouse. The current (baseline) situation has only the grid supplying the HPWH controlled by a digital thermostat. Despite this being the normal mode of control/operation, it is far from optimal from a daily operational point of view. In addition, this intervention develops an integration of wind and PV generators in order to reduce energy cost.

The sampling time $t_s = 30$ minutes giving the final sampling interval $N = 48$. The average inlet cold water temperature[4], T_{in}, in Port Elizabeth in early winter is shown in Figure 2. A typical winter day is chosen so as simulate the worst case scenario with the highest thermal demand period in South Africa. However, for precise economic estimation of the payback (break-even) period, simulations are done based on selected days in each season; summer, autumn, winter and spring in the case study. This accounts for the changing seasonal hot water demand and variation of inlet cold water temperature that directly affect the annualised energy and cost savings calculated in 4.6

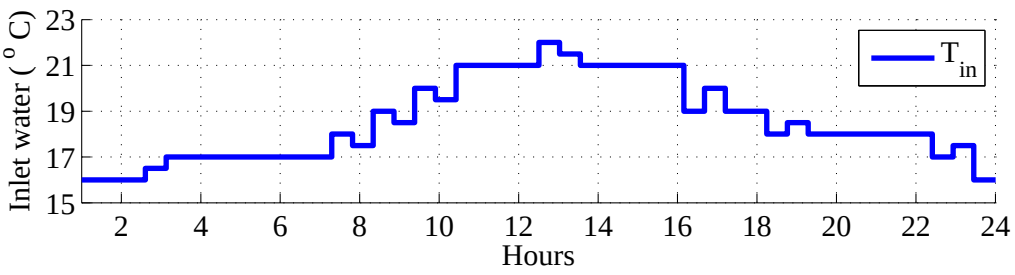

Figure 2: Hourly inlet cold water temperature

The hot water demand flow rate $W_D(k)$ is shown in Figure 3. There is no hot water usage between 00:00-05:00 and 22:00-00:00 mainly because the occupants are asleep during these periods. Because of

[4]http://www.wunderground.com/weather-forecast/ZA/Port_Elizabeth.html?MR=1

lack of accurate hot water demand data from the case study, the average hot water demand used here is in agreement with that of Meyer [38, 39] in an experiment conducted in South Africa for a town house, except that the farmhouse does not use hot water in the early and late hours of the day. The preferred hot water temperatures are set to $55\,^{\circ}\text{C} \leq T_k \leq 65\,^{\circ}\text{C}$; the average country ambient temperature of $T_a = 25\,^{\circ}\text{C}$ is used. The initial water temperature is set to $T_o = 60\,^{\circ}\text{C}$. However, the above desirable temperature varies from one individual to another.

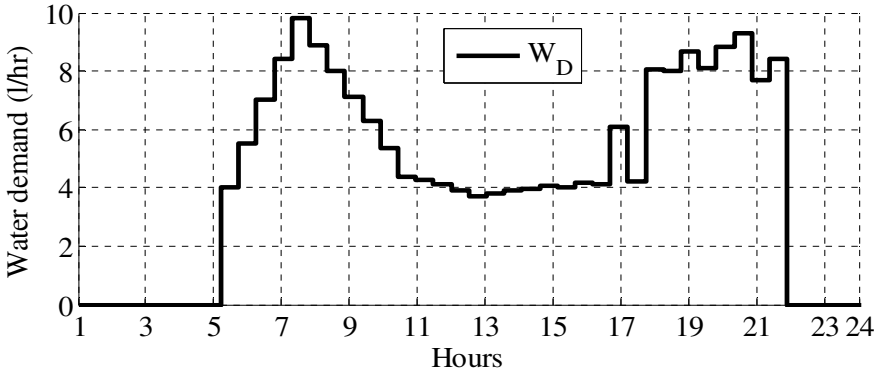

Figure 3: Flow rate of hot water in winter

3.4.1. Heat pump water heater parameters

The HPWH type is an air source tank-wrapped condenser coil, with following the parameters shown in Table 1.

Table 1: Heat pump parameters

Power input (kW)	COP	Storage capacity (l)	Compressor (cc)	Tank (h/ø) (m)	$\triangle x\,(m)$	$\kappa\,(W/m.K)$	$h\,(W/m^2K)$
6	3.8	270	39.0	1.41×0.66	0.035	0.055	6.3

3.4.2. Wind generator parameters

The wind generator's technical specifications are given Table 2 . In this paper, η_t is the mechanical gearbox efficiency only. However, the overall wind-to-turbine power convention coefficient or the Betz limit C_p is factored in as well.

Table 2: Wind generator parameters

Maximum power (kW)	$\eta_t\,(\%)$	$\eta_g\,(\%)$	$\rho_a\,(kg/m^3)$	C_p	$A_w\,(m^2)$
3.5	0.9	0.8	1.22	0.48	11.3

The hourly wind speed at Port Elizabeth[5] is presented in Figure 4 below:

[5]http://www.timeanddate.com/weather/south-africa/port-elizabeth/hourly

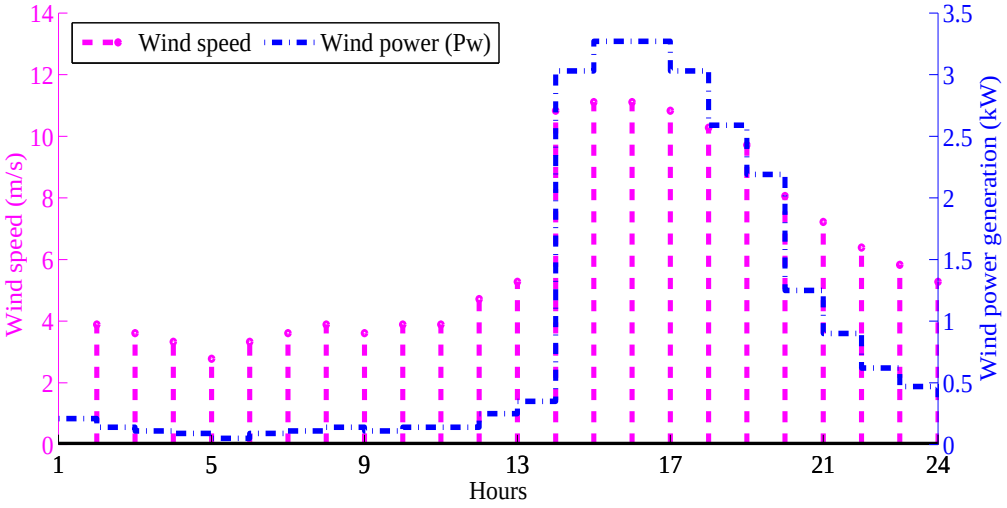

Figure 4: Wind power output and speed for Port Elizabeth

The PV power is input data in this model, measured in the case study. In South Africa the PV feed-in tariff [6] is $3.94R/kWh$, whereas for wind it is $1.25R/kWh$.

4. Simulation results and discussion

4.1. Optimal heat pump switching control strategy in winter

In Figure 5 optimal control turns *on* the HPWH supply switch from 00:00 to 01:00 in the morning; thereafter, it keeps it *off* between 01:00-04:00. However, in order to avoid operating in peak TOU, the OC turns *on* after 04:00 to heat the water in advance to meet the hot water demand, which starts at 05:30, shown in Figure 3, using cheaper off-peak energy. It turns *off* again towards 07:00, avoiding the standard TOU tariff to save energy cost. The HPWH is *off* till 16:00, when it turns *on* again to heat the water before the evening peak period, as a load-shifting strategy. Subsequently, after evening peak it only comes *on* for 30 minutes to preheat the water. The OC finally turns *off* at 21:30 because the hot water demand W_d, Figure 3, declines to zero and the temperature is still above T_{low}, shown in Figure 7.

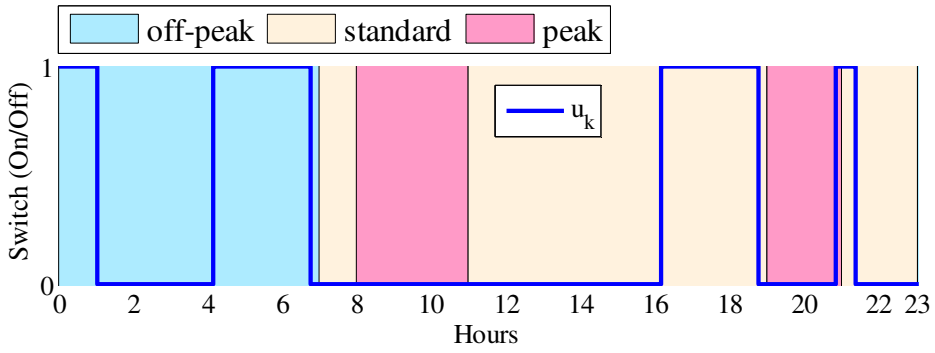

Figure 5: Optimal heat pump power supply switching

The OC shows the ability to predict the demand and TOU accurately in order to save energy cost through load shifting, overcoming the limitation of a digital thermostat control strategy used in most HPWHs, as shown in 4.3. The TOU electricity tariff legend in Figure 5 applies to all figures in this paper.

[6] https://energypedia.info/wiki

4.2. Optimal grid and feed-in power supply strategy in winter

The results of the OC power scheduling are presented in Figure 6, showing wind power P_w, PV power P_{pv}, grid power P_g and HPWH P_{hp} demand. The grid power assumes negative values during feed-in and positive ones when supplying the HPWH load. In Figure 6, P_g supplies the HPWH from midnight to 01:00, with very little supplement from wind power P_w. The slight deviation between HPWH demand P_{hp} and P_g is due to the low amount of power supplied by the wind generator. The grid stops supplying power between 01:00 and 04:00 because the HPWH is *off*, as shown in Figure 5, and has begun accepting a little wind power. At 04:00 the OC resumes grid power supply till 06:30 and at this time the PV power generation P_{pv} starts increasing power feed-in into the grid.

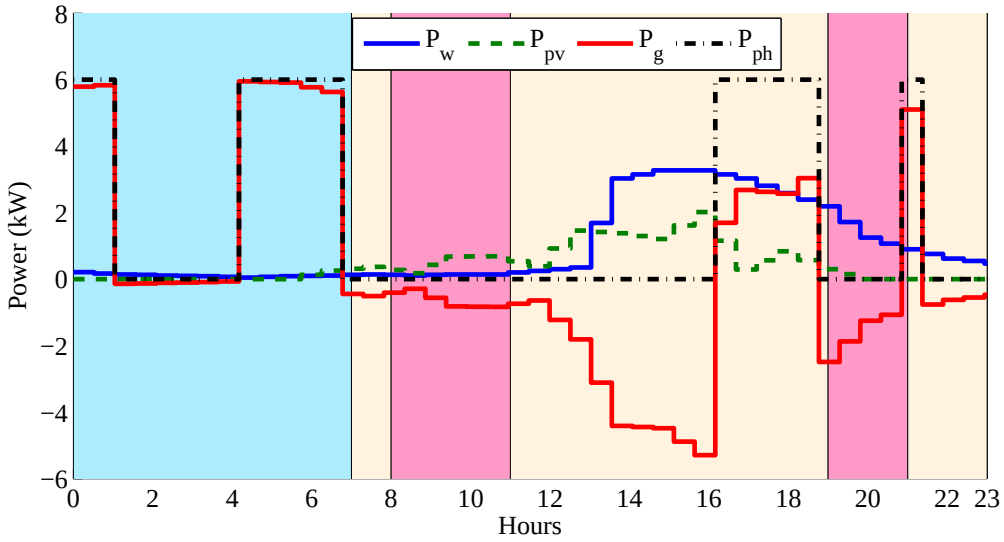

Figure 6: Optimal grid and renewable power scheduling strategy

From 07:00 the OC continues power feed-in to the grid till 16:00. At 16:00, the combined wind and PV power is unable to meet the HPWH demand, causing the OC to bring in P_g to supplement the deficit. The OC opts to use the cheap renewable power whenever available to supply the HPWH in order to reduce the energy cost. It manages to schedule load-shifting and avoid using peak TOU expensive energy, giving a cost benefit to the end-user.

4.3. Comparison between optimal and digital thermostat control strategies

Figure 7 shows the hot water demand flow rate, optimal and digital thermostat switching and lastly the hot water temperature T_k, which is the state variable. The OC switches *on* the HPWH from 00:00 - 01:00; the hot water temperature rises gradually from the initial $T_o = 60\,^{\circ}\text{C}$ to $61.5\,^{\circ}\text{C}$. The temperature stays almost constant between 01:00 and 04:30 with very little drop caused by convectional losses. However, in Figure 7 the temperature appears constant merely because of axis scaling; the half-hour temperature between 01:00 and 04:30 clearly shows a marginal fall due to standby losses; $61.4726\,^{\circ}\text{C}$, $61.4725\,^{\circ}\text{C}$, $61.4724\,^{\circ}\text{C}$, $61.4724\,^{\circ}\text{C}$, $61.4723\,^{\circ}\text{C}$, $61.4722\,^{\circ}\text{C}$ and $61.4721\,^{\circ}\text{C}$ respectively. The limited hot water temperature drop in the absence of flow rate is due to good tank insulation in the case study.

The HPWH again turns *on* at 04:00, causing the water temperature to rise. The non-linear T_k rise is due to the resumption of hot water demand causing inlet of cold water into the tank. The temperature after 07:00 shows a steady decline mainly because of the hot water consumption trend. At the same time the HPWH switches *off*, so the decline in T_k is caused by the inlet of cold water to balance the volume as a result of hot water demand. The OC turns *on* the HPWH at 16:00 to preheat the water before evening peak TOU, effectively shifting the load. The OC shows the capability of predicting the right time to turn *on* the HPWH so that the end-user is not inconvenienced and has hot water available at the right temperature.

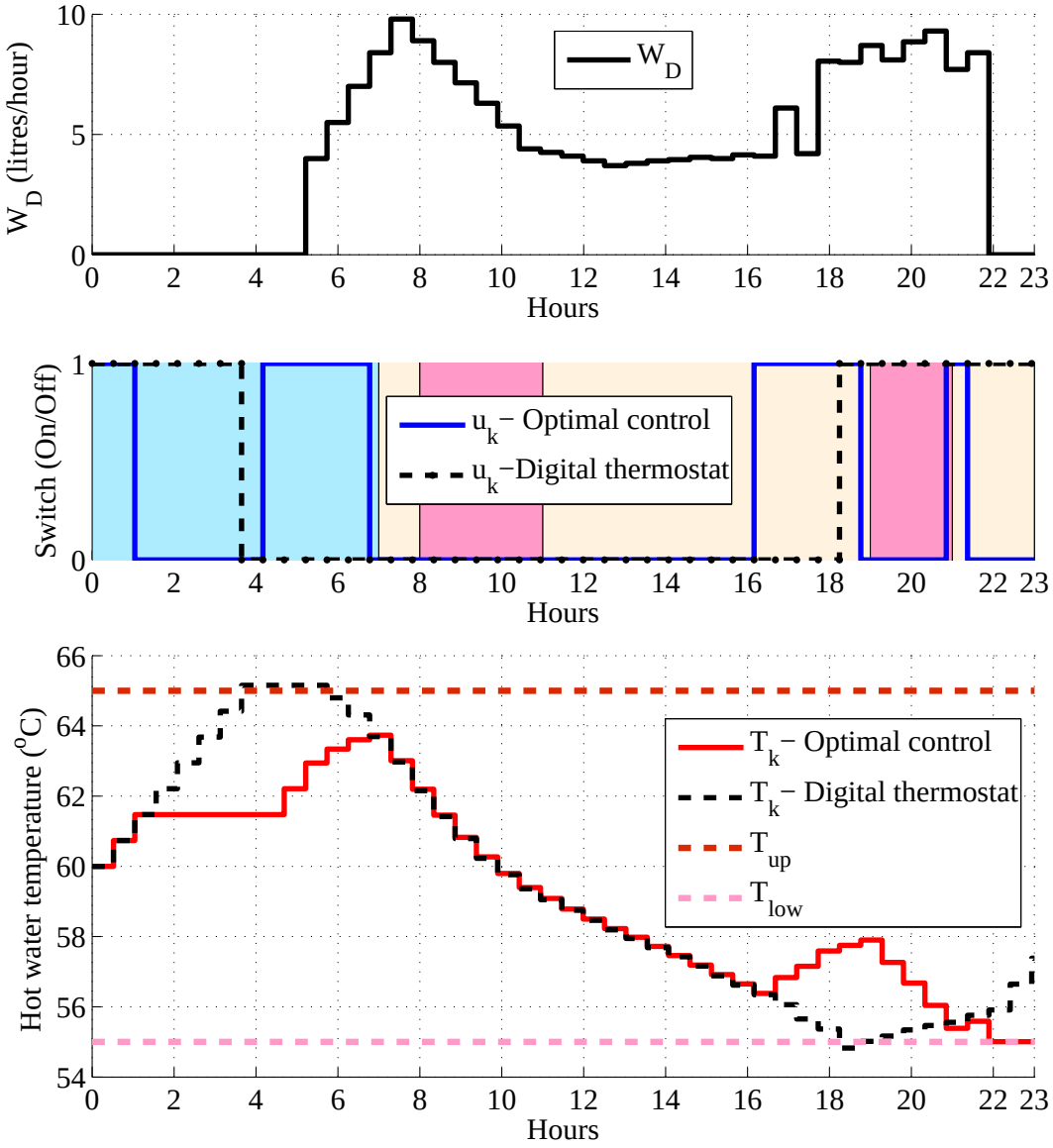

Figure 7: Hot water temperature's dependency on switching and water usage

The baseline situation is as well simulated to compare the benefits of OC over a digital thermostat control strategy, which is used in most HPWHs on the market. As shown in Figure 7, the digital thermostat (u_k − digital thermostat) turns *on* the HPWH from midnight till 03:30 when T_k hits the upper set point, regardless of whether there is demand for hot water or not, using more energy. At 18:00 the thermostat turns *on* upon T_k dropping below the lower desirable limit. Since it has no capability to shift load it runs through peak TOU, incurring huge energy cost. In the study the switching *on* frequencies over the control horizon were 13 and 20 for optimal and digital thermostat control respectively. The OC has a lower switching frequency, which saves on energy and prolongs the compressor's life cycle.

However, it is worth pointing out that the desired temperature should not be set so high, beyond the rated capacity of the HPWH, as it will never reach that required temperature when demand for hot water occurs. A realistic temperature should be set within the range of the HPWH power rating, else the end-user has to raise the water temperature inside the tank beforehand by some other means (e.g. by using an in-line resistive element heater).

4.4. Baseline and optimal energy savings in winter

Table 3 shows the daily energy and cost saving: baseline (digital thermostat control strategy), and opti-

mal control strategy. The baseline is the current situation in the case study, where the 6 kW HPWH operates on the digital thermostat control strategy and is supplied by the grid alone. The optimal cost is the energy cost after implementation of this intervention. The DREs power is treated as free energy or benefit in the case study upon implementation of this intervention. The feed-in energy is the total PV and wind power injected into the utility grid, except the power consumed by the load.

Table 3: Daily optimal energy savings

Baseline (kWh/day)	Optimal (kWh/day)	Total feed-in (kWh/day)	Baseline cost (R/day)	Optimal cost (R/day)	Energy saving (%)	Cost saving (%)
144.00	29.26	14.62	48.83	14.29	85.67	70.74

The OC strategy yields 85.67% on energy saving owing to a substantial benefit from wind and PV free energy that meets the HPWH load. Hence the proposed model is a near net-zero-energy building. A cost saving of 70.74% is realised, implying that this model has the potential to be cost-effective with the revenue from DREs sales.

4.5. Effects of seasonal hot water demand variation on optimal temperature

The model is further simulated on a selected day in each of the four seasons to account for the varying hot water demand given in the case study as shown in Figure 8. The changing hot water demand shows an effect on the optimal energy and cost saving, because of the different scheduling strategy. Many factors affect the consumption of hot water such as behavioral, social, ambient and inlet water temperatures. The simulation is run in each season to account consumption factor in order to accurately determine the optimal cost and energy savings. The savings; optimal benefit and DREs sales are further averaged over the season and annualized for the calculation of break-even period in subsection 4.6

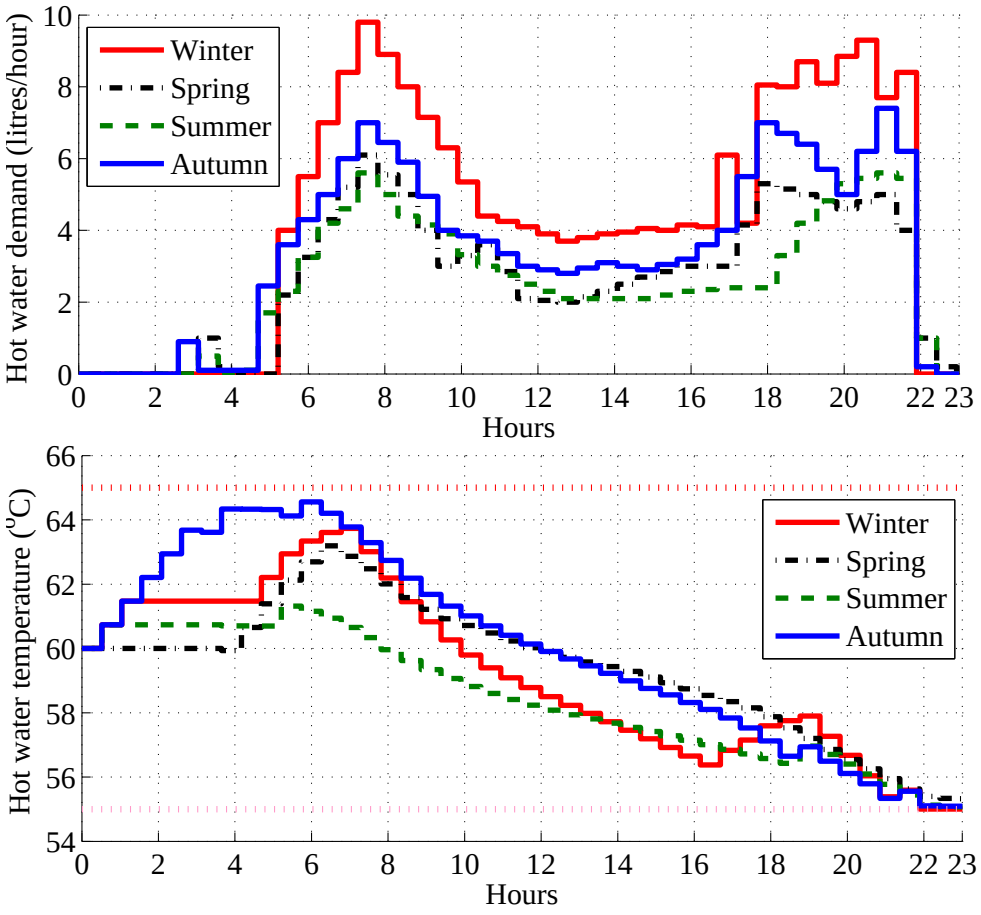

Figure 8: Effects of seasonal hot water demand on optimal water temperature

The optimal hot water temperature is relatively similar in each season because of the similarity in the hot water usage in the house. In Figure 8, autumn T_k steadily rises above other seasons due to the hot water consumption which starts earlier around 02:30 making the OC to turn *on* the HPWH before the hot water demand. There is reduction in the switching *on* frequency in the afternoons in most seasons owing to the improved inlet water temperature. However, in a typical situation, people still bath the same frequency regardless of the season, but what reduces is the hot water requirement for mixing during a bath owing to the improved ambient temperatures.

4.6. Break-even period analysis

In order to ascertain the economic viability of this model, the payback period is calculated based on DREs sales and OC benefit which reflect the difference between baseline and optimal energy costs due to the OC intervention. Table 4 below shows the revenue from solar energy sales, wind energy sales and OC benefit. The simulation is run in each season to account for demand variation, then the costs/revenue of that day is averaged over the season and annualized to reflect an average amount per annum. The energy cost saved after intervention is translated as a benefit cost to the end-user.

The payback period is calculated making the assumptions that the solar sales, wind sales, cost saving, operation and maintenance costs will remain constant throughout the period, as well a discount factor or interest rate of 4.4% for February 2015 in the case study is used to reflect the time value of money. The 4.4% is indicative of the inflation rate in South Africa. Though, it is expected that there would be an increase in all these factors, it cannot be reliably estimated at this time. Thus, the discounted present value (DPV)[7]

[7]https://en.wikipedia.org/wiki/Discounted-cash-flow

for one year's cash flow in one future period is given in equation (44) below:

$$DPV = \frac{FV}{(1+r)^n}, \tag{44}$$

where:

DPV - is the discounted present value of the future cash flow (FV)
FV - is the nominal value of a cash flow amount in a future period
r - is the interest rate or discount rate, which reflects the cost of tying up capital and may also The allow for the risk that the payment may not be received in full
n - is the time in years before the future cash flow occurs.

values in brackets indicate the money spent, which presents a negative cash flow and the amounts are in South African Rand.

Table 4: Discounted cash flows

Years :	0	1	2	3	4	5
Solar photovoltaic	(27 500.00)					
Wind generator	(23 500.00)					
Controllers	(22 900.00)					
Inverters and accessories	(15 000.00)					
Installation cost	(14 000.00)					
Maintenance cost	(2 500.00)	(2 500.00)	(2 500.00)	(2 500.00)	(2 500.00)	(2 500.00)
Wind sales	6 638.66	6 638.66	6 638.66	6 638.66	6 638.66	6 638.66
Solar sales	13 568.47	13 568.47	13 568.47	13 568.47	13 568.47	13 568.47
Optimal benefits	12607.10	12607.10	12607.10	12607.10	12607.10	12607.10
	(102 900.00)	30 314.24	30 314.24	30 314.24	30 314.24	30 314.24
Discount factor @4.4%	1.00	0.96	0.92	0.88	0.84	0.81
Discounted cash flows	(102 900.00)	29 036.63	27 812.86	26 640.67	25 517.88	24 442.42

Table 5: Discounted payback period

Years	Discounted cash flows	Cumulative cash flows
0	(102 900.00)	(102 900.00)
1	29 036.63	(73 863.37)
2	27 812.86	(46 050.51)
3	**26 640.67**	**(19 409.84)**
4	25 517.88	6 108.04
5	24 442.42	30 550.46

According to Table 5 the payback period is 3 years and 9 months. The break-even period is shorter owing to the optimal benefits. The money generated from the feed-in sales can still assist to offset the power utility bills. Therefore, this optimal switching control has benefit for those intending to transform their homes into cost-effective and net-zero energy buildings in countries with an attractive feed-in tariff.

5. Conclusions

The TOU based optimal switching control shows the potential to save energy cost, as well as energy-not-delivered on the utility side, thus a reduction on primary inputs and greenhouse gases. This model yields a maximum energy saving of 85.67% and has the potential to be cost-effective on energy bills. This intervention provides a practical optimal integration of wind and other DREs into homes, with the benefit of energy trade-off and the possibility of achieving a net zero-energy building.

The economic analysis shows a payback period of 3 years and 9 months. There are other incentives pertaining to rebates on HPWH, wind power and solar PV application that are not considered in this paper, which are evident in the case study and could further lower the payback period.

This model is suitable for application in both peri-urban and rural areas, in the generation of hot water, space heating and renewable energy integration. However, there is a need for future research into the application of a predictive control model incorporating other renewable sources, such as biomass and fuel cells. It can be adopted by home-owners who want to integrate renewable energy sources using energy-efficient equipment such as HPWH to save energy with the minimum environmental impact. The OC strategy offers the potential to be cost-effective and to overcome the limitations of digital thermostat control used in most heat pumps on the market.

Acknowledgements

The authors would like to thank the National Research Foundation (NRF) of South Africa grant NRF SFH14080687344, Maastricht University under (MUNDO) NICHE ZMB 037, The University of Zambia and the National Hub for Energy Efficiency and Demand Side Management (EEDSM) for financial and other support for this research.

References

[1] M. M. Rahman, M. Rasul, M. M. K. Khan, Energy conservation measures in an institutional building in sub-tropical climate in australia, Applied Energy 87 (10) (2010) 2994–3004.

[2] H. Esen, M. Inalli, M. Esen, Technoeconomic appraisal of a ground source heat pump system for a heating season in eastern turkey, Energy Conversion and Management 47 (10) (2006) 1281 – 1297.

[3] K. Chua, S. Chou, W. Yang, Advances in heat pump systems: A review, Applied Energy 87 (12) (2010) 3611–3624.

[4] T. Chow, Y. Bai, K. Fong, Z. Lin, Analysis of a solar assisted heat pump system for indoor swimming pool water and space heating, Applied Energy 100 (2012) 309–317.

[5] M. Esen, T. Yuksel, Experimental evaluation of using various renewable energy sources for heating a greenhouse, Energy and Buildings 65 (0) (2013) 340 – 351.

[6] N. Roonprasang, P. Namprakai, N. Pratinthong, Experimental studies of a new solar water heater system using a solar water pump, Energy 33 (4) (2008) 639–646.

[7] J. Tamasauskas, M. Poirier, R. Zmeureanu, R. Sunyé, Modeling and optimization of a solar assisted heat pump using ice slurry as a latent storage material, Solar Energy 86 (11) (2012) 3316–3325.

[8] X. Zhang, X. Zhao, J. Xu, X. Yu, Characterization of a solar photovoltaic/loop-heat-pipe heat pump water heating system, Applied Energy 102 (2013) 1229–1245.

[9] J. Ji, G. Pei, T.-t. Chow, W. He, A. Zhang, J. Dong, H. Yi, Performance of multi-functional domestic heat-pump system, Applied Energy 80 (3) (2005) 307–326.

[10] I. Lane, N. Beute, A model of the domestic hot water load, Power Systems, IEEE Transactions on 11 (4) (1996) 1850–1855.

[11] Y. Tian, C.-Y. Zhao, A review of solar collectors and thermal energy storage in solar thermal applications, Applied Energy 104 (2013) 538–553.

[12] R. Rankin, P. G. Rousseau, M. van Eldik, Demand side management for commercial buildings using an inline heat pump water heating methodology, Energy conversion and management 45 (9) (2004) 1553–1563.

[13] S. M. Sichilalu, X. Xia, Optimal energy control of grid tied pv–diesel–battery hybrid system powering heat pump water heater, Solar Energy 115 (2015) 243–254.

[14] A. Mellit, M. Benghanem, S. Kalogirou, Modeling and simulation of a stand-alone photovoltaic system using an adaptive artificial neural network: Proposition for a new sizing procedure, Renewable Energy 32 (2) (2007) 285 – 313.

[15] W. Kellogg, M. Nehrir, G. Venkataramanan, V. Gerez, Optimal unit sizing for a hybrid wind/photovoltaic generating system, Electric Power Systems Research 39 (1) (1996) 35 – 38.

[16] T. Khatib, A. Mohamed, K. Sopian, Optimization of a pv/wind micro-grid for rural housing electrification using a hybrid iterative/genetic algorithm: case study of kuala terengganu, malaysia, Energy and Buildings 47 (2012) 321–331.

[17] C. Nayar, S. Phillips, W. James, T. Pryor, D. Remmer, Novel wind/diesel/battery hybrid energy system, Solar Energy 51 (1) (1993) 65 – 78.

[18] T. Mathaba, M. Mpholo, M. Letuma, Velocity and power density analysis of the wind at letšeng-la-terae in lesotho, Renewable Energy 46 (2012) 210–217.

[19] M. Moghavvemi, M. Ismail, B. Murali, S. Yang, A. Attaran, S. Moghavvemi, Development and optimization of a pv/diesel hybrid supply system for remote controlled commercial large scale fm transmitters, Energy Conversion and Management 75 (2013) 542–551.

[20] Y. Zhao, Y. Lu, C. Yan, S. Wang, Mpc-based optimal scheduling of grid-connected low energy buildings with thermal energy storages, Energy and Buildings 86 (2015) 415–426.
[21] W. Zeiler, G. Boxem, Net-zero energy building schools, Renewable Energy 49 (0) (2013) 282 – 286.
[22] P. A. Torcellini, D. B. Crawley, Understanding zero-energy buildings, ASHRAE Journal 48 (9) (2006) 62–69.
[23] S. C. Bengea, R. A. Decarlo, Optimal control of switching systems, automatica 41 (1) (2005) 11–27.
[24] S. Sichilalu, X. Xia, J. Zhang, Optimal scheduling strategy for a grid-connected photovoltaic system for heat pump water heaters, Energy Procedia 61 (2014) 1511–1514.
[25] X. Sun, Y. Dai, V. Novakovic, J. Wu, R. Wang, Performance comparison of direct expansion solar-assisted heat pump and conventional air source heat pump for domestic hot water, Energy Procedia 70 (0) (2015) 394 – 401.
[26] M. Mehrpooya, H. Hemmatabady, M. H. Ahmadi, Optimization of performance of combined solar collector-geothermal heat pump systems to supply thermal load needed for heating greenhouses, Energy Conversion and Management 97 (0) (2015) 382 – 392.
[27] K. Kusakana, Operation cost minimization of photovoltaic–diesel–battery hybrid systems, Energy 85 (2015) 645–653.
[28] C. Fraga, F. Mermoud, P. Hollmuller, E. Pampaloni, B. Lachal, Large solar driven heat pump system for a multifamily building: Long term in-situ monitoring, Solar Energy 114 (0) (2015) 427 – 439.
[29] C. Verhelst, D. Degrauwe, F. Logist, J. Van Impe, L. Helsen, Multi-objective optimal control of an air-to-water heat pump for residential heating, Building Simulation 5 (3) (2012) 281–291. doi:10.1007/s12273-012-0061-z.
[30] L. Paull, H. Li, L. Chang, A novel domestic electric water heater model for a multi-objective demand side management program, Electric Power Systems Research 80 (12) (2010) 1446–1451.
[31] M. Ranaboldo, B. Domenech, G. A. Reyes, L. Ferrer-Martí, R. P. Moreno, A. García-Villoria, Off-grid community electrification projects based on wind and solar energies: A case study in nicaragua, Solar Energy 117 (2015) 268–281.
[32] M. Kim, M. S. Kim, J. D. Chung, Transient thermal behavior of a water heater system driven by a heat pump, International journal of refrigeration 27 (4) (2004) 415–421.
[33] J. Zhang, X. Xia, Best switching time of hot water cylinder-switched optimal control approach, in: AFRICON 2007, IEEE, 2007, pp. 1–7.
[34] K. Khan, M. Rasul, M. M. K. Khan, Energy conservation in buildings: cogeneration and cogeneration coupled with thermal energy storage, Applied Energy 77 (1) (2004) 15–34.
[35] M. Gustafson, J. Baylor, G. Epstein, Direct water heater load control-estimating program effectiveness using an engineering model, Power Systems, IEEE Transactions on 8 (1) (1993) 137–143.
[36] P. Dolan, M. Nehrir, V. Gerez, Development of a monte carlo based aggregate model for residential electric water heater loads, Electric Power Systems Research 36 (1) (1996) 29–35.
[37] S. Ashok, Optimised model for community-based hybrid energy system, Renewable energy 32 (7) (2007) 1155–1164.
[38] J. P. Meyer, A review of domestic hot-water consumption in south africa, R&D Journal 16 (2000) p55–61.
[39] J. Meyer, M. Tshimankinda, Domestic hot water consumption in south african townhouses, Energy Conversion and Management 39 (7) (1998) 679–684.